Journal of Catalysis 264 (2009) 93–103

Contents lists available at ScienceDirect

Journal of Catalysis

journal homepage: www.elsevier.com/locate/jcat

Etching of the intermetallic compounds PdGa and Pd_3Ga_7: An effective way to increase catalytic activity?

Kirill Kovnir [a,b,*], Jürgen Osswald [a], Marc Armbrüster [b,*], Detre Teschner [a], Gisela Weinberg [a], Ute Wild [a], Axel Knop-Gericke [a], Thorsten Ressler [a,1], Yuri Grin [b], Robert Schlögl [a]

[a] Fritz Haber Institute of the Max Planck Society, Faradayweg 4-6, 14195 Berlin, Germany
[b] Max-Planck-Institut für Chemische Physik fester Stoffe, Nöthnitzer Str. 40, 01187 Dresden, Germany

ARTICLE INFO

Article history:
Received 11 November 2008
Revised 10 March 2009
Accepted 14 March 2009
Available online 26 April 2009

Keywords:
Intermetallic compounds
PdGa
Pd_3Ga_7
Active-site isolation
Chemical etching
Palladium
Gallium
Selective hydrogenation
Acetylene
In situ XPS

ABSTRACT

The structurally ordered intermetallic compounds PdGa and Pd_3Ga_7 constitute highly selective catalysts for the selective semi-hydrogenation of acetylene. The milling of as-synthesized samples, followed by etching with ammonia solution increased the activity of the catalysts by factor of 60. Chemically etched samples possess high activity and simultaneously keep their high selectivity. Chemical analysis confirms that the etching procedure is mostly specific to gallium species, thus less affecting the palladium. Detailed investigations reveal the influence of the chemical etching on the morphology and surface of the particles. As a result of the etching, nano-caverns are formed (SEM and BET), and the surface is enriched in palladium (XPS and EDX), while the bulk crystal structure is not affected (XRD). The mechanism and applicability of the etching procedure is discussed in view of the active-site isolation concept.

1. Introduction

The chemical industry permanently demands improved catalysts to decrease production costs and save natural resources. A lot of phenomenological data concerning reactions pathways, intermediates, side-reactions, and the formation of by-products have been accumulated during the last century. Generalization of these data allows formulation of the requirements for improved catalysts. But the rational synthesis of novel catalysts is still not well developed, lacking detailed understanding of the processes and knowledge-based new concepts.

Recently, we have introduced structurally well-ordered intermetallic compounds as catalysts led by the concept of active-site isolation [1–5]. The employed intermetallic compounds possess metallic conductivity, a well-defined crystal structure as well as partly covalent bonding between the atoms. Consequently, these intermetallic compounds have a very important advantage compared to conventional alloys: the atomic environment of the catalytically active metal is fixed by the realized crystal structure while in alloys the random distribution of the atoms leads to a number of possible adsorbate configurations on the catalytically active metal. This advantage results not only in a very homogeneous distribution of the active sites in intermetallic compounds but also the phenomenon of segregation is significantly reduced or not present at all due to the covalent bonding between the transition metal and the main groups elements stabilizing the active centers (see e.g. [1,6]). Furthermore, the covalent bonding modifies the electronic states of the active metal, which have a high impact on the catalytic properties [1].

To verify the suggested concept the partial hydrogenation of acetylene to ethylene ($C_2H_2 + H_2 \rightarrow C_2H_4$, $\Delta H = -172$ kJ/mol) was chosen as test reaction. Because acetylene poisons the ethylene polymerization catalysts, the acetylene content in the ethylene feed has to be reduced from ~1% to the low ppm range [7,8]. Moreover, economic efficiency requires a high selectivity of the catalyst – especially in the presence of ethylene excess – to prevent the hydrogenation of ethylene to ethane. Typical hydrogenation catalysts contain metallic palladium dispersed on metal oxides [7,8]. The main drawbacks, such as deactivation and low selectivity of these catalysts, are widely discussed in the literature [7–12].

* Corresponding authors. Present address: Department of Chemistry and Biochemistry, Dittmer Bldg., Florida State University, Tallahassee, FL 32306, USA. Fax: +1 850 6448281 (K. Kovnir); +49 351 46464002 (M. Armbrüster).
E-mail addresses: kkovnir@chem.fsu.edu (K. Kovnir), research@armbruester.net (M. Armbrüster).
[1] Present address: Institute of Chemistry, Technical University Berlin, Straße des 17. Juni 135, 10623 Berlin, Germany.

0021-9517/$ - see front matter © 2009 Elsevier Inc. All rights reserved.
doi:10.1016/j.jcat.2009.03.007

According to the suggested concept, the structurally well-ordered intermetallic compounds PdGa [13] and Pd_3Ga_7 [14] were chosen to prove the active-site isolation concept. In PdGa the palladium atoms are isolated by the surrounding gallium atoms forming a single-capped distorted trigonal prism (Fig. 1). The shortest Pd–Pd distance is 3.01 Å. In contrast, the gallium atoms in Pd_3Ga_7 are arranged in paired square antiprisms, resulting in a Pd–Pd separation of 2.73 Å within the pair of antiprisms. The shortest Pd–Pd distance between the Pd atoms of two different pairs is 4.27 Å (Fig. 1). It was shown, that these intermetallic compounds possess high structural stability in different atmospheres as well as high selectivity and long-term stability in the selective acetylene hydrogenation [1–4].

However, the use of unsupported intermetallic compounds as hydrogenation catalysts results in a low activity per gram of catalyst, but as advantage, the obtained results can be attributed to a single active compound with well-defined crystal structure. Surface characterization of PdGa and Pd_3Ga_7 by X-ray photoelectron spectroscopy (XPS) as well as ion scattering spectroscopy [4] revealed the presence of gallium oxides on the surface of the particles. To increase the catalytic activity a chemical etching procedure with ammonia solution was successfully introduced, aiming at the selective removal of the inactive gallium oxides [5].

Here we report a detailed investigation of the impact of chemical etching on the catalytic properties, the chemical composition of the surface and the particle morphology, which is an important step toward the efficient use of intermetallic compounds as catalysts. Furthermore, the applicability of the chemical etching to intermetallic compounds as catalysts is discussed.

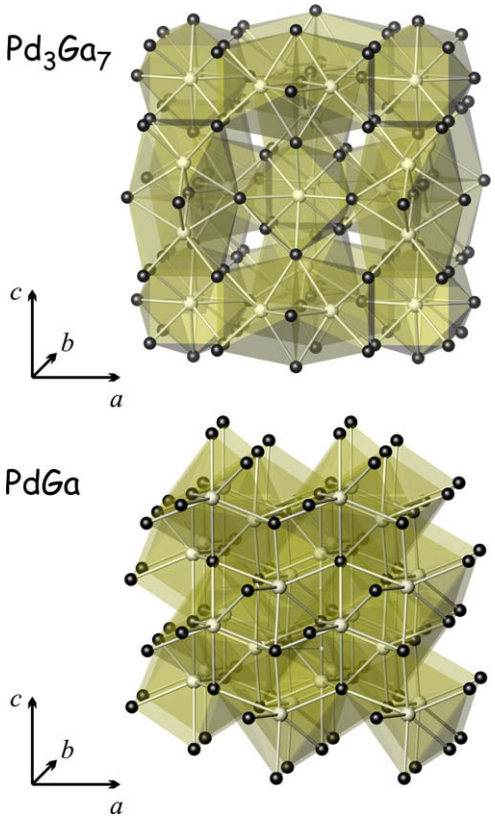

Fig. 1. Crystal structures of Pd_3Ga_7 (top) and PdGa (bottom). Pd: white spheres; Ga: black spheres. Each palladium atom in PdGa is coordinated by seven gallium atoms, while in Pd_3Ga_7 eight gallium atoms are surrounding the Pd atoms as indicated by polyhedra.

2. Experimental

2.1. Sample preparation

The intermetallic compound PdGa was prepared using elemental Pd (ChemPur, 99.95%) and Ga (ChemPur, 99.99%) as starting materials. The elements were weighted in 1:1 molar ratios in air and subsequently transferred to a glove box filled with argon (O_2 and H_2O < 1 ppm). The mixture was placed in a glassy carbon crucible and slowly heated up in a high-frequency induction furnace (Hüttinger TIG 5/300, 30 A, 200 V, 30 to 300 kHz). After the exothermic reaction of the elements the melt was annealed for 10 min before the oven was switched off, thus allowing the samples to cool down to ambient temperature. In order to reach thermodynamic equilibrium, the ingots of PdGa were enclosed in evacuated quartz glass ampules and annealed at 1073 K for one week. Pd_3Ga_7 was prepared similarly by using a 3:7 molar ratio of the components. The obtained ingots expanded during cooling and disintegrated into a fine, gray powder. The powder was pelleted prior to annealing at 673 K for four weeks. After annealing samples were quenched in water, crushed, and investigated by X-ray powder diffraction revealing single phase sample.

2.2. Milling

To increase the surface area, 1 g of a coarsely crushed sample was milled in a closed 4 ml tungsten carbide (WC) mortar using two WC balls. The milling was performed in a swing mill (Retsch MM 200, 25 Hz) for 2×30 min for PdGa and 2×10 min for Pd_3Ga_7. In each case, different samples were milled in air as well as under argon. For the latter the WC mortar was loaded in a glove box and sealed with air tight tape.

2.3. Etching procedure

Commercial ammonia solution (Merck, 25% p.a.) was diluted with distilled water to the required pH values. Measurements of pH were performed with a Knick pH-Meter 761 Calimatic equipped with a Mettler-Toledo Inlab 422 electrode. The instrument was calibrated with buffer solutions (Merck centiPUR, pH 7.0 and 9.0). Fifty milligrams of air-milled PdGa or Pd_3Ga_7 were added to 75 ml of the diluted ammonia solution and stirred for 10 min at ambient temperature. The suspension was filtered and the residue was washed with an additional 75 ml of the solution while the filtrate was chemically analyzed. The etched samples were dried by evacuation to 10 mbar for at least 60 min in a desiccator. Throughout this manuscript, a set of abbreviations is used: **Pd_3Ga_7_milled**, **Pd_3Ga_7_10.5**, *etc.* The first letters name the intermetallic compound, Pd_3Ga_7 or PdGa, while the last digits indicate the pH value of the etching solution used for preparation of the sample; "milled" corresponds to samples used as obtained from the ball-milling procedure in air without further etching. Also the terms "soft" and "strong" etching are used throughout this paper: soft etching corresponds to samples etched at the *lowest* pH 9.0 applied for both PdGa and Pd_3Ga_7, while strong etching corresponds to samples etched at the *highest* pH values used, 9.8 and 10.5 for PdGa and Pd_3Ga_7, respectively.

2.4. X-ray powder diffraction

X-ray powder diffraction (XRD) experiments were performed in transmission mode. Samples were finely ground and spread on a 6 μm thick Mylar foil coated with vaseline. For the measurements a Gunier camera (Huber G670, image plate, Cu Kα_1 radiation with λ = 1.540562 Å) was utilized.

2.5. Chemical analysis

Chemical analysis of the filtrate after etching was performed by inductively coupled plasma-optical emission spectrometry (ICP-OES) with a Varian Vista RL spectrometer. All values are the averages of at least three replicates.

2.6. Surface area measurements

Adsorption–desorption measurements of N_2 using a Quantachrome Quantasorb Jr. have been performed to determine the surface area of the intermetallic compounds by the multipoint Brunauer–Emmett–Teller (BET) method. The samples (~2 g) were pretreated (20 ml/min He, 393 K, 12 h) and measurements were performed by determining the total amount of nitrogen adsorbed using three different nitrogen concentrations.

Milled (in air) samples of PdGa and Pd_3Ga_7 possessed a surface area below the nitrogen BET detection limit and were re-measured using krypton as adsorbate (BELSORP-max). The milled samples (400 mg) were pretreated in vacuum at 373 K for 1 h and measurements were performed by determination of the total amount of Kr adsorbed using seven different krypton concentrations.

2.7. X-ray photoelectron spectroscopy (XPS)

X-ray photoelectron spectroscopy was performed with an UHV system equipped with a Leybold LHS 12 MCD energy analyzer and further with XPS surface analysis tools. The samples for the measurements were prepared from milled and etched PdGa and Pd_3Ga_7 powder. XPS data were obtained using Al Kα radiation (1486.6 eV) and a pass energy of 48 eV resulting in a spectrometer resolution of 1.1 eV. The elemental composition of the near-surface region was estimated – after satellite subtraction and Shirley background correction – by integration of the peak areas and applying the corresponding sensitivity factors [15]. The gallium content was calculated from Ga2$p_{3/2}$, palladium from the sum of Pd3$d_{3/2}$ and Pd3$d_{5/2}$ and carbon from the C1*s* peak area. The oxygen concentration was derived from the O1*s* peak area corrected for the Pd3$p_{3/2}$ contribution. The Pd3$p_{3/2}$ peak area was calculated from Pd3*d* one using a factor of 2.9 for the (Pd3*d*)/(Pd3$p_{3/2}$) ratio [4,15].

2.8. In situ X-ray photoelectron spectroscopy (in situ XPS)

In situ high-pressure X-ray photoelectron spectroscopy (XPS) experiments were performed at beamline U49/2-PGM1 at BESSY (Berlin, Germany). Details of the setup have been published earlier [16]. Briefly, the photoelectron spectrometer system uses a differentially pumped lens system between the sample cell and the electron analyzer, allowing XPS investigations during catalytic conditions in the mbar pressure range. For the measurements dense pills of **Pd_3Ga_7_9.8** and **Pd_3Ga_7_10.5** (8 mm in diameter, 1 mm thick) were produced by pressing the powders at room temperature in stainless steel pressing tools. XPS investigations were performed in UHV (10^{-8} mbar) and under *in situ* conditions: 1.0 mbar of H_2 (Westfalen Gas, 99.999%) and 0.1 mbar of C_2H_2 (solvent free, Linde, 99.6%) at 375 to 400 K. Prior to UHV investigations the samples were sputtered with Ar^+ ions to clean the surface from possible contaminations. An *in situ* experiment included introduction of the gases at room temperature, equilibration for 15 min, heating the sample to the corresponding temperature with 10 K/min rate and, equilibration for another 15 min, afterwards the XP spectra were recorded. Pd3*d*, Ga3*p*, Ga3*d*, and C1*s* XP spectra were recorded with varying the wavelength of the incoming radiation resulting in photoelectrons with similar kinetic energy. Thus, the same information depth was probed for the different core levels. Three different kinetic energies were chosen – 780, 380, and 150 eV. These correspond to information depths (three-times the inelastic mean free path) of ~4.5, 3, and 2 nm, respectively, for clean Pd_3Ga_7 [17]. Element concentrations were determined from Pd3*d*, Ga3*p*, and C1*s* peak areas. Gas-phase analysis was carried out using a quadrupole Balzers mass spectrometer connected by a leak valve to the experimental cell. Ion currents corresponding to acetylene (m/e = 26), ethylene (m/e = 27) and ethane (m/e = 30) were monitored. For the evaluation, the ion currents of ethylene and ethane were normalized to the acetylene signal and plotted versus time of the experiment. The normalization was performed to account for possible pressure fluctuations.

2.9. Scanning electron microscopy (SEM)

Scanning electron microscopy (SEM) was performed with a Hitachi S4800 with a cold FEG (Field Emission Gun). The setup was equipped with an Energy Dispersive X-ray system EDAX Genesis 4.52, the EDX detector consists of Si(Li) crystal and a SUTW (Super Ultra Thin Window). Samples were mounted on Al-holder with conducting carbon tape.

2.10. Catalysis

A detailed description of the catalysis experiments has been published elsewhere [4]. Catalytic investigations of the selective hydrogenation of acetylene were performed within a plug flow reactor (30 mL/min) with excess of ethylene: 0.5% acetylene, 5% hydrogen (99.999%), and 50% ethylene (99.95%) in helium (99.999%). Pre-mixed acetylene in helium (2%) (C_2H_2: 99.6% solvent free, He: 99.996%) was used. All gases were supplied by Westfalen Gas (Germany). A Varian CP 4900 MicroGC (Gas Chromatograph) was used for the exhaust gas analysis during isothermal experiments. As reference, commercial Pd/Al_2O_3 (5 wt.%, Aldrich) with a BET surface area of 114 $m^2\,g^{-1}$ and an active metal surface of 5.6 $m^2\,g^{-1}$ (determined by CO chemisorption) was used [3,4]. Catalytic data for both reference catalysts presented in Fig. 3 were obtained under the same reaction conditions as the data of the intermetallic catalysts for comparison purposes.

Selectivity and conversion were calculated by the following formulas [4]:

$$conversion = \frac{C_{feed} - C_x}{C_{feed}} \times 100\%;$$

$$selectivity = \frac{C_{feed} - C_x}{C_{feed} - C_x + C_{ethane} + 2C_{C_4H_x}} \times 100\%,$$

where C_{feed} is the acetylene concentration in the feed, C_x is the acetylene concentration after the reactor, C_{ethane} is the ethane concentration, and $C_{C_4H_x}$ is the total concentration of the different C_4H_x hydrocarbons detected. To measure the selectivity at similar conversion, different amounts of catalyst were used according to their specific activity determined in previous experiments. The activity of the samples was calculated using the following equation:

$$activity = \frac{conversion \cdot C_{feed} \cdot C_{ex}}{100\% \cdot m_{Pd}},$$

where m_{Pd} is the amount of Pd in the catalyst in gram and C_{ex} is 1.904 g/h. The latter was introduced to convert the acetylene flow from [ml/min] to [g/h] and is based on the ideal gas model:

$$C_{ex} = \frac{M_{acetylene} \cdot p \cdot F}{R \cdot T},$$

where $M_{acetylene}$ is the molar weight of acetylene (26 g/mol), p the pressure (1.013 bar), F the total gas flow through the reactor at room temperature (1.8 l/h at 300 K), R the universal gas constant R (8.3144 J $mol^{-1}\,K^{-1}$), and T the temperature (300 K).

3. Results and discussion

3.1. Milling

The milling procedure has significant influence on the catalytic activity of the investigated compounds. Milling of the intermetallic compounds PdGa and Pd_3Ga_7 was performed with the aim to increase the catalysts surface area. Initially the milling was performed in air. Afterwards, significant covering of the surface of the catalyst milled in air by gallium oxides was detected by XPS and SEM [4,5]. Since all the syntheses were performed in a glove box (O_2 and H_2O contents lower than 1 ppm), it is very unlikely that the oxygen contamination was caused by the preparation. Although gallium oxides were detected, the activity was considerably increased after milling the samples, e.g. by a factor of 20 for PdGa.

To avoid oxide formation, the milling procedure was performed in inert argon atmosphere. Surprisingly, samples milled under argon showed negligible activity compared to the ones milled in air. Moreover, the particles after milling in Ar stuck to each other, which hindered regrinding of the samples in a mortar, while air-milled samples could easily be reground. Apparently, during the argon milling a partial destruction of the surface occurred and segregation of gallium (melting temperature 303 K) took place, thus leading to sticking of the particles. Milling the samples in air leads to a partial oxidation of the surface of gallium and the formed gallium oxides prevent the particles from sticking together. Because of their higher catalytic activity, the following investigations were carried out on air-milled samples.

Chemical etching with ammonia solution was employed to remove the gallium oxide overlayer from the surface of the intermetallic particles. Ammonia solutions are well known for chemical etching of semiconductor surfaces such as GaAs [18–20]. Chemical etching of PdGa and Pd_3Ga_7 was performed at room temperature with an aqueous ammonia solution at pH values as indicated. After drying, the samples were catalytically characterized (Fig. 2 and Table 1).

3.2. Catalysis

First we will discuss the influence of the etching on Pd_3Ga_7 before turning our attention to PdGa. As reference, the sample **Pd_3Ga_7_milled** with a mass of 50 mg was measured and showed a conversion of 70% in steady-state regime, as well as a selectivity toward ethylene of 79% (activity 0.3 $g_{C_2H_2}/g_{Pd}$ h). The activity of the samples etched at high pH values after 20 h time on stream was significantly increased: 20.5 and 15.7 $g_{C_2H_2}/g_{Pd}$ h for **Pd_3Ga_7_10.2** and **Pd_3Ga_7_10.5**, respectively. The employed mass could significantly be reduced by a factor of 62.5 and 50, compared to **Pd_3Ga_7_milled**, still revealing high conversion levels of 97% and 94%, respectively, after the first 30 min. In contrast to the milled sample the long-term stability was reduced. Nonetheless, after 20 h time on stream the etched samples still revealed higher conversion (65%) than Pd supported on alumina (43%, see Fig. 2). Concerning the selectivity, the samples etched at high pH values did not reach a steady-state. During 20 h of experiment, their selectivity continuously increased – a process that seems to be closely related with the deactivation of these catalysts. Catalysts etched at low pH values (**Pd_3Ga_7_9.5** and **Pd_3Ga_7_9.0**) were less active but were more stable than the ones etched at high pH values. **Pd_3Ga_7_9.0** showed a stable conversion level of 97% during the 20 h time on stream, while the activity increased by a factor of six (1.8 *vs.* 0.3 $g_{C_2H_2}/g_{Pd}$ h for **Pd_3Ga_7_9.0** and **Pd_3Ga_7_milled**, respectively). The samples etched at low pH values 9.0 and 9.5 reached a steady-state selectivity of 50% to 55% after the first 5 to 8 h (Fig. 2), which is significantly higher than the selectivity of the reference catalyst Pd/Al_2O_3 – 17%.

Similar results were obtained for the intermetallic compound PdGa (Fig. 2). **PdGa_9.8** and **PdGa_9.0** showed high activity (9.6 and 2.9 $g_{C_2H_2}/g_{Pd}$ h, respectively) compared to the milled sample (0.3 $g_{C_2H_2}/g_{Pd}$ h). In contrast to Pd_3Ga_7, etching of PdGa has minor impact on the long-term stability of the compounds. The selectivity of the PdGa samples decreases in the sequence **PdGa_milled** (74%)–**PdGa_9.0** (64%)–**PdGa_9.8** (56%), *viz.* with increasing pH.

The activity–selectivity relationship for the intermetallic catalysts PdGa and Pd_3Ga_7 is presented in Fig. 3. Both compounds exhibit a performance outside the parameter range given by the reference catalysts – unsupported $Pd_{20}Ag_{80}$ [4] and 5 wt.% Pd/Al_2O_3. The PdGa and Pd_3Ga_7 families of catalysts were characterized by conversion-selectivity trends running in parallel to that of the reference Pd catalysts but with intrinsically higher selectivity.

To summarize, chemical etching significantly enhanced the catalytic activity of Pd–Ga intermetallic compounds. While soft etching increased the activity of PdGa and Pd_3Ga_7 by a factor of 9 and 6, respectively, strong etching resulted in an increase of up to 60 times. Softly etched intermetallic catalysts showed high stability – similar to milled samples – while strongly etched samples experienced significant deactivation. After 20 h time on stream all intermetallic samples were still much more stable and selective than Pd supported on alumina, which only showed a selectivity of 15% and significant deactivation from 97% to 43% conversion. The following XPS, XRD, BET, SEM, EDX, and *in situ* XPS measurements as well as the chemical analysis of the etching solution were performed to understand the ongoing processes during the chemical etching.

3.3. Analysis after chemical etching

The ammonia solution after the etching procedure was filtered and palladium and gallium concentrations were determined by ICP-OES (Table 2). The amount of dissolved gallium strongly depends on the pH value of the etching solution, while palladium is practically not dissolved. Strong etching dissolves more than 10 mol.% of the gallium, while soft etching leaches significantly lower amounts of gallium (around 0.4 mol.%).

3.4. XPS

To determine the near-surface composition, XPS measurements were performed on milled, strongly etched (pH 10.5 and 9.8 for Pd_3Ga_7 and PdGa, respectively) and softly etched samples (pH 9.0 for both compounds). The results of the XPS investigations are collected in Table 3. In the case of PdGa etching leads to the expected decrease in gallium and oxygen contents, while the relative palladium content in the near-surface region increases. It should be noted that for strongly etched PdGa samples the Pd/Ga ratio was close to 2:1, which does not correspond to the bulk composition, verifying the partial dissolution of gallium from the intermetallic compound. In addition, the surface concentration of carbon increased with increasing pH of the etching solution. This indicates the formation of a significant amount of fresh and reactive palladium sites on the surface, which readily adsorbed carbon-containing species from the air. The removal of the gallium oxide coating during the etching procedure results in a lower oxygen concentration for the etched samples.

For Pd_3Ga_7 the general tendency is similar: the strongly etched sample **Pd_3Ga_7_10.5** showed less gallium and oxygen and more palladium in the near-surface region compared to the milled samples. As in the case of PdGa, the palladium content on the surface was higher than expected from the bulk composition: the Pd/Ga

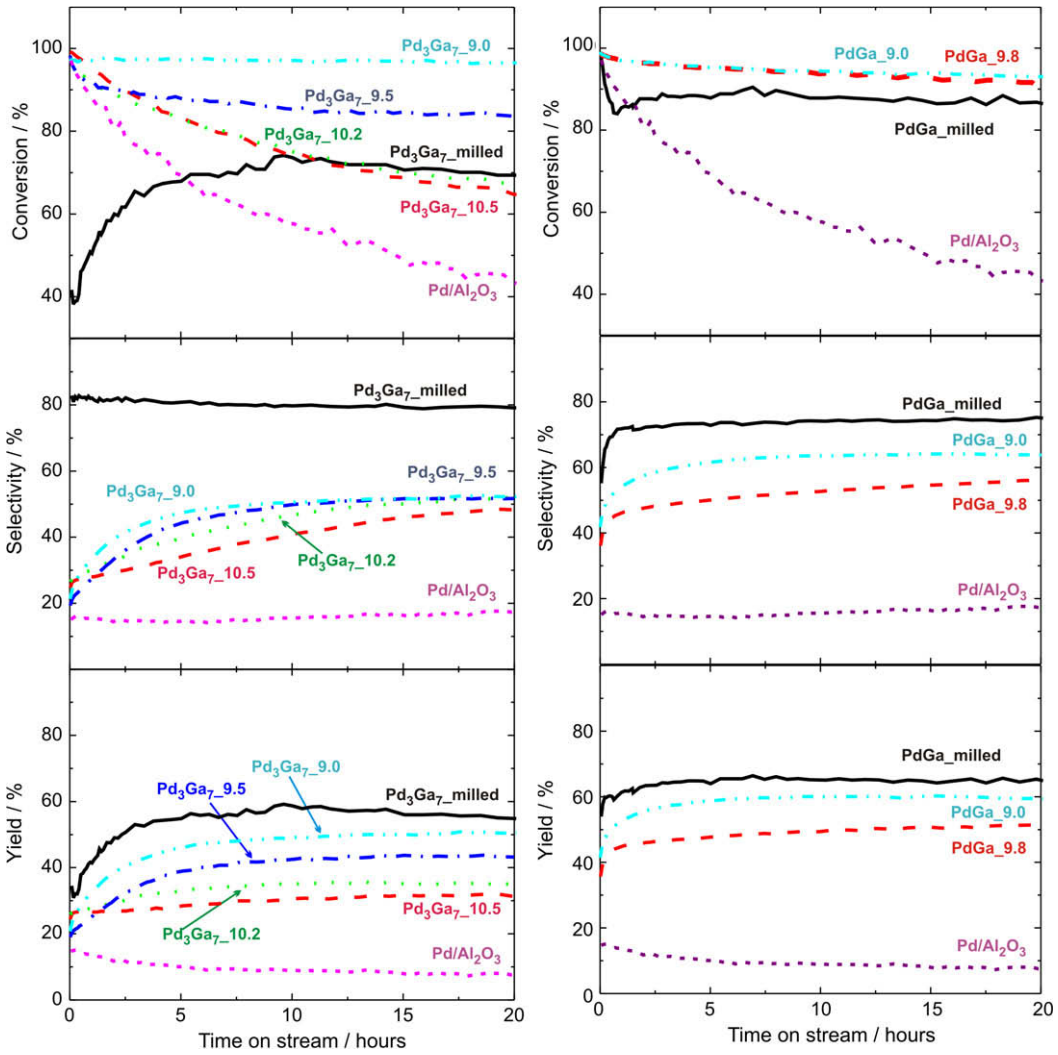

Fig. 2. Acetylene conversion (top), selectivity (middle) and ethylene yield (bottom) for milled and etched samples of Pd_3Ga_7 (left) and PdGa (right). Sample weights: **Pd_3Ga_7_milled** – 50 mg, **Pd_3Ga_7_10.5** – 1 mg, **Pd_3Ga_7_10.2** – 0.8 mg, **Pd_3Ga_7_9.5** – 5.5 mg, **Pd_3Ga_7_9.0** – 13 mg; **PdGa_milled** – 40 mg, **PdGa_9.8** – 1.5 mg, **PdGa_9.0** – 5 mg. For comparison the data of a commercial 5 wt.% Pd/Al_2O_3 (0.15 mg) is also shown. Feed composition: 0.5% C_2H_2 + 5% H_2 + 50% C_2H_4 + 44.5% He; isothermal experiments at 473 K.

Table 1
Acetylene conversion, selectivity, and activity of milled and chemically etched PdGa, Pd_3Ga_7, and the reference catalyst Pd/Al_2O_3 after 20 h time on stream in a mixture of 0.5% C_2H_2 + 5% H_2 + 50% C_2H_4 in helium at 473 K.

Sample	Sample mass (mg)	Conversion (%)	Selectivity (%)	Activity ($g_{C_2H_2}/g_{Pd}$ h)
Pd_3Ga_7_milled	50	69	79	0.3
Pd_3Ga_7_9.0	13.0	97	52	1.8
Pd_3Ga_7_9.5	5.50	84	52	3.7
Pd_3Ga_7_10.2	0.80	68	52	20.5
Pd_3Ga_7_10.5	1.00	65	48	15.7
PdGa_milled	40.0	86	75	0.3
PdGa_9.0	5.00	93	64	2.9
PdGa_9.8	1.50	91	56	9.6
Pd/Al_2O_3	0.15	43	17	545.8

ratio was ~4:7 instead of 3:7. For the softly etched sample (**Pd_3Ga_7_9.0**) this effect is not so pronounced, particularly the oxygen and palladium concentrations in the near-surface region were similar to **Pd_3Ga_7_milled**, while the etching resulted in a decrease in the gallium and an increase in the carbon concentration.

The amount of gallium dissolved during strong etching (10 at.%) cannot originate solely from dissolving the surface gallium oxides. XPS clearly reveals that strong etching leads not only to the dissolution of gallium oxides from the catalyst surface but also to a partial destruction of the intermetallic surface resulting in an palladium enrichment, thereby locally disrupting the well-ordered crystal structure. In the case of soft etching the surface gallium oxide layers are preferentially dissolved, while the intermetallic structure is only little affected.

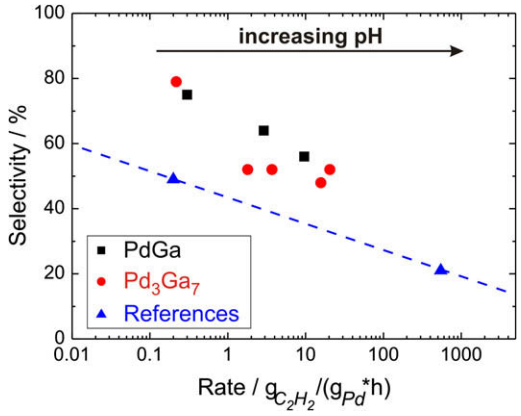

Fig. 3. Selectivity to ethylene in percentage *vs.* the rate of acetylene hydrogenation. Data for milled and differently etched PdGa (squares) and Pd_3Ga_7 (circles) catalysts are shown together with two reference catalysts (triangles): unsupported Pd–Ag alloy (left) and 5 wt.% Pd/Al_2O_3 (right) [4]. Damaging of the intermetallic compounds is expressed in the reduction in the maximum performance when the etching solution becomes too strong resulting in an Pd-enrichment of the surface.

Table 2
ICP-OES analysis of the filtered solution after etching of PdGa and Pd_3Ga_7.

Sample	Pd (mg/L)	Ga (mg/L)	Corresponds to	
			mol.% Pd	mol.% Ga
Initial NH_3solution	<0.1	<0.02	–	–
PdGa_9.0	<0.1	1.0(1)	–	0.4
PdGa_9.8	~0.06	5.5(2)	0.02	2.1
Pd_3Ga_7_9.0	<0.1	1.2(1)	–	0.3
Pd_3Ga_7_10.5	0.35(6)	46.6(5)	0.13	11.6

Table 3
Near-surface concentration (at.%) for milled and etched samples of PdGa and Pd_3Ga_7 obtained by XPS analysis. Estimated relative error of the concentrations is in the region of 20%.

Sample	Ga	O[a]	C	Pd
PdGa_milled	32	57	5	6
PdGa_9.0	26	48	14	12
PdGa_9.8	14	36	17	32
Pd_3Ga_7_milled	36	58	4	2
Pd_3Ga_7_9.0	26	56	17	2
Pd_3Ga_7_10.5	27	48	10	16

[a] Although the values for the oxygen content may not be absolutely accurate, they should be sufficient to evaluate the trends since the same fitting procedure was applied for all investigated samples.

These results are in excellent agreement with the observed catalytic behavior of the investigated samples. The decreasing selectivity of etched PdGa and Pd_3Ga_7 with increasing pH values of the etching solution can be explained by partial leaching of gallium from the intermetallic compound. This caused the partial destruction of the crystal structure, thus partly annihilating the isolation of active Pd sites and leading to the formation of palladium ensembles on the surface. Accordingly, this results in a decreased selectivity as well as reduced long-term stability. Increasing the pH of the etching solution causes stronger destruction of the intermetallic surface and more pronounced palladium agglomeration. The extreme case of palladium clustering results in formation of metallic Pd which possesses low selectivity and strong deactivation, as in the case of Pd/Al_2O_3.

3.5. XRD, SEM, and BET

Comparison of the powder X-ray diffraction patterns of as-synthesized, milled, and etched samples revealed clearly that milling leads to a significant decrease in the crystallite size (from 60 nm to 14 nm), as can be seen from the broadening of the diffraction peaks (Fig. S1). In turn, diffraction patterns of the etched samples revealed a slightly higher crystallite size as the milled samples (22 nm). Thus, chemical etching did not lead to a further decrease in the crystallite size. However, BET measurements showed a significant gain in surface area of strongly etched samples, compared to the milled samples (Table 4).

To understand the reason for the surface area increase, the particle morphology was investigated by high-resolution SEM. No substantial changes in particle size distribution or shape took place and no agglomeration of the particles occurred for the etched samples. Conventional EDX analysis revealed a stoichiometric composition for the milled and softly etched samples, while strongly etched samples possessed a slight palladium excess in agreement with the chemical analysis of the etching solution. High-resolution SEM showed a strong influence of the chemical etching procedure on the particle surface. Comparison of images of milled, softly and strongly etched samples of PdGa and Pd_3Ga_7 clearly revealed the formation of small pores with a diameter of 20 to 50 nm after the etching (Figs. 4 and 5), which was more pronounced in the case of strong etching. The relatively small increase in specific surface area (2 to 4 times, Table 4) and absence of hysteresis loop on the isotherms for etched samples indicated that the formed pores are not infinite, they rather corresponded to some kind of closed caverns formed during the etching. Thus, instead of decreasing the particle size, a system of caverns was created, leading to higher surface area while at the same time gallium oxides were partly removed. Upon increasing the pH of the etching solution the gain in surface area increased.

While activities calculated per gram of catalyst showed a strong increase for the etched samples (Table 1) it is more meaningful to compare the activity per active Pd surface. By taking into account CO chemisorption data [3,4] the corresponding activity for the reference catalyst Pd/Al_2O_3 is 4.9 $g_{C_2H_2}$ m_{Pd}^{-2} h^{-1}. Unfortunately, the absence of detectable CO chemisorption on the milled samples did not allow to determine the concentration of active Pd surface atoms [4]. However, a rough estimate can be made by using the BET surface area and the XPS Pd near-surface concentration (Tables 3 and 4). For milled samples of PdGa and Pd_3Ga_7, the activities per "surface Pd" are 8 $g_{C_2H_2}$ m_{Pd}^{-2} h^{-1} and 16 $g_{C_2H_2}$ m_{Pd}^{-2} h^{-1}, respectively. For strongly etched samples the activity indeed increases up to 18 $g_{C_2H_2}$ m_{Pd}^{-2} h^{-1} for both **PdGa_9.8** and **Pd_3Ga_7_10.5**. This clearly shows that the increasing activity of the etched samples is mainly caused by a combination of the higher surface area and the higher surface Pd concentration. However, an intrinsic activity increase, e.g. by forming more active Pd ensembles cannot be excluded. The presented data also demonstrate that the activity of intermetallic catalysts is comparable with the activity of supported Pd catalysts.

Detailed investigations were performed with Pd_3Ga_7 for the two extreme pH values of the etching solution: 10.5 and 9.0. The micrographs shown in Figs. 4 and 5 were taken with an accelerating voltage (V_{acc}) of 5 kV in SE (Secondary Electrons) mode to get

Table 4
Specific surface areas obtained from nitrogen (etched samples) and krypton (milled samples) adsorption BET measurements.

Sample	Surface area (m^2/g)
PdGa_milled	0.41(2)
PdGa_9.0	~0.5(2)
PdGa_9.8	1.0(2)
Pd_3Ga_7_milled	0.37(2)
Pd_3Ga_7_9.0	~0.5(2)
Pd_3Ga_7_10.5	2.2(2)

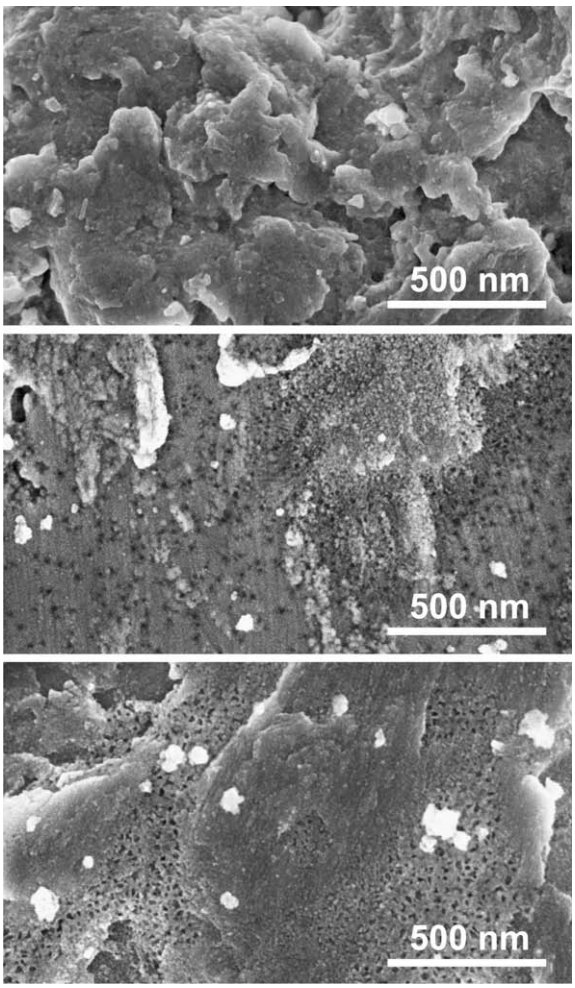

Fig. 4. High-resolution SEM pictures (5 keV, SE) of the surface of PdGa: milled (top), chemically etched at pH 9.0 (middle), and at pH 9.8 (bottom).

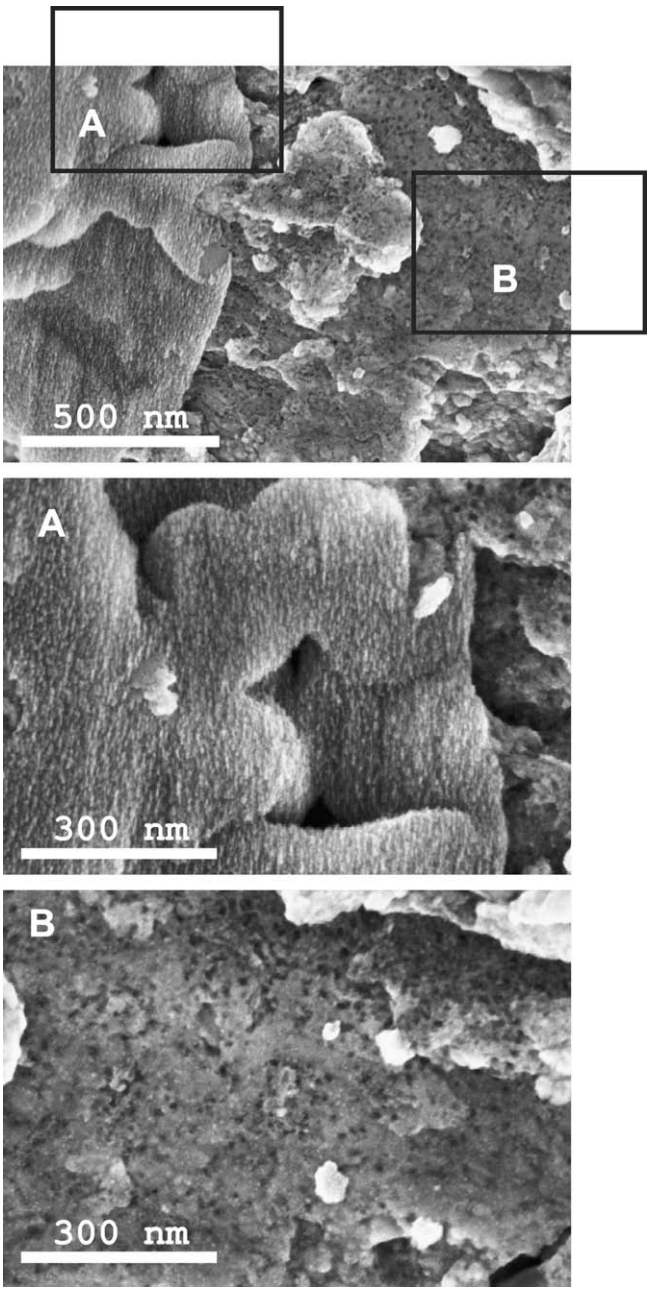

Fig. 5. High-resolution SEM picture (5 keV, SE) of the surface of Pd_3Ga_7, chemically etched at pH 9.0 (top) where two different kinds of areas were detected. Magnified view of the rough area of the top picture corresponds to frame A (middle), magnified view of the smooth area of the top picture corresponds to frame B (bottom).

information on the surface region of the catalysts. SE information depth is generally about 10 nm. Image shown in Fig. 6 was taken with V_{acc} = 1.5 kV in a mixed SE/BSE (Back Scattered Electrons) mode to get information on the near surface in addition to the element contrast. BSE information depth adds up to about 35 nm under these conditions.

High-resolution SEM investigations of the surface of the sample **Pd_3Ga_7_9.0** revealed that softly etched samples contain two different types of surface: more smooth ones containing caverns and more rough ones without them (Fig. 5). EDX analysis performed (information depth ~200 nm) indicated that the smooth areas are richer in palladium and carbon, while the rough areas contain more gallium and oxygen (Table 5). Accordingly to the EDX analysis, smooth areas correspond to intermetallic surface with relatively high palladium and additional carbon content, while the rough areas correspond to a remaining gallium oxide overlayer.

Investigations of the strongly etched sample **Pd_3Ga_7_10.5** by high-resolution SEM also revealed the presence of two different surface types (Fig. 6): dark-gray areas, and light-gray areas containing caverns. For the dark-gray areas EDX analysis revealed a composition close to the smooth areas of the sample **Pd_3Ga_7_9.0**. In turn, light-gray porous areas showed an excess of palladium and carbon (Table 5), indicating the formation of a palladium-rich overlayer on the surface of intermetallic compound.

It should be noted that the results presented in Table 5 are only semi-quantitative as no standards were applied. However, comparing results obtained from different areas and samples is still useful. Furthermore, the SEM results correlate well with the XPS data – strong etching leads to a significant disturbance of the catalyst surface and accumulation of carbon on the surface, while the intermetallic surface was less affected by soft etching. In both cases the gallium oxides coatings were not fully removed.

3.6. In situ XPS

The same two samples (**Pd_3Ga_7_9.0** and **Pd_3Ga_7_10.5**) investigated by SEM were chosen for a detailed *in situ* synchrotron-based XPS investigation. This technique allows monitoring the chemical composition of the surface with higher surface sensitivity and

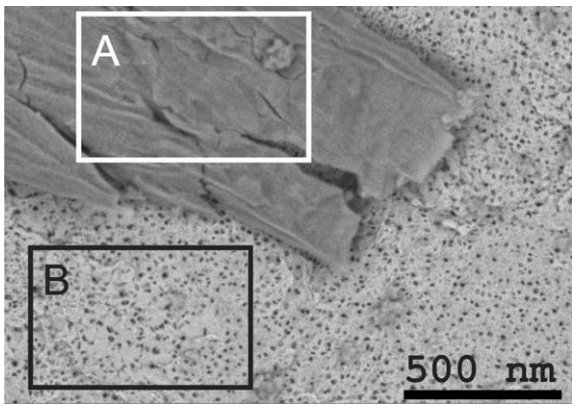

Fig. 6. High-resolution SEM picture (1.5 keV, SE/BSE) of the surface of Pd_3Ga_7 chemically etched at pH 10.5, where two different kinds of areas can be seen (A: dark gray, no caverns; B: light gray, caverns).

Table 5
Chemical composition (at.%) obtained from EDX analysis (V_{acc} = 5 kV, information depth ~200 nm) for the different areas of the samples **Pd_3Ga_7_9.0** and **Pd_3Ga_7_10.5** corresponding to the frames marked in Figs. 5 and 6. Estimated relative error of the concentration is in the region of 20%.

Frame	Ga	O	C	Pd	Ratio Pd:Ga
Pd_3Ga_7_9.0					
Rough area (Fig. 5, frame A)	41	40	11	8	1:5
Smooth area (Fig. 5, frame B)	30	21	25	24	1:1
Pd_3Ga_7_10.5					
Dark-gray area (Fig. 6, frame A)	27	30	16	26	1:1
Light-gray area (Fig. 6, frame B)	13	7	32	47	4:1

the introduction of gas phase during surface analysis. A significant amount of carbon was detected on the surface of each compound in UHV conditions, which is typical for active Pd catalysts investigated in this setup [21]. The detected carbon might originate from the residual pressure of hydrocarbons present in the cell used for *in situ* investigations at mbar conditions. XP spectra were collected prior to and during the reaction semi-hydrogenation of acetylene. The gas composition was monitored by mass-spectrometry and the plots of the normalized ion currents during the experiments are presented in Fig. S2. The desired product of the reaction is ethylene (m/e = 27), while the main by-product is ethane (m/e = 30). Both investigated samples are active and selective for the hydrogenation of acetylene.

C1*s* spectra before and during the reaction for both investigated samples are shown in Fig. 7. The binding energy of the main carbon peak (at 284.5 to 284.7 eV) changed slightly when switching from UHV to reaction conditions and can be assigned to graphitic carbon [21,22]. During the reaction an additional carbon component appeared at higher binding energy, fitted as a broad peak with a maximum at 288.6 eV and a FWHM > 2 eV. Contribution of the gas phase carbon in both cases was significantly smaller (less than 2%), as indicated on the upper-left plot in Fig. 7. The high binding energy carbon components corresponded to a mixture of the aliphatic hydrocarbon polymers $(CH_2)_n$ (~285 eV) and, mainly, oxygenated carbon species, containing C–O bonds (286 to 288 eV) [22,23]. Apparently, C–O bonds were formed due to the reaction of the feed with Ga oxides (see description of Ga3*d* spectra). The amount of aliphatic and oxygenated hydrocarbons was significantly higher for the strongly etched sample (**Pd_3Ga_7_10.5**), demonstrating its higher ability to produce such carbonaceous deposits – most probably due to higher content of non-isolated Pd atoms on the surfaces. This finding explains why the strongly etched samples do not possess high long-term stability: here, as in the case of elemental palladium, the accumulation of polymerized carbon leads to covering of the surface, thus deactivating the catalyst.

A significant difference between strongly and softly etched samples can be observed when examining the Pd3*d* spectra (Fig. 8). The UHV spectrum of **Pd_3Ga_7_9.0** shows a narrow (FWHM = 0.77 eV) single peak with a binding energy of 336.4 eV which corresponds to the binding energy of the Pd3*d* peak (336.4 eV) for the as-synthesized Pd_3Ga_7 intermetallic compound, measured as reference. During hydrogenation the Pd3*d* peak became broader (FWHM = 0.94 eV) but remained at the same binding energy. On the other hand, the UHV Pd3*d* spectrum of the strongly etched **Pd_3Ga_7_10.5** is a superposition of two components with binding energies of 336.3 eV (30%) and 335.7 eV (70%, Fig. 8). The first one corresponds to the intermetallic compound Pd_3Ga_7, while the second component can be attributed to a more Pd-rich phase, for example Pd_2Ga [25,26]. It should be noted that the binding energy is still higher than for elemental Pd with 335.0 eV [21,24]. Thus, in the near-surface region of **Pd_3Ga_7_10.5** two different kinds of Pd are present: isolated and mainly non-isolated ones. In the depth profiling experiment the variation of the wavelength of the incoming radiation allowed to receive information from different penetration depths (see experimental Section 2.8). Depth profiling of **Pd_3Ga_7_10.5** revealed that the additional component is not only present in the topmost layers but also present in the deeper layers (Fig. 9).

Both investigated samples revealed a high stability of the surface under reaction conditions. Even in the case of strongly etched **Pd_3Ga_7_10.5**, containing two different kinds of Pd species on the surface, the surface seemed to be preserved during acetylene

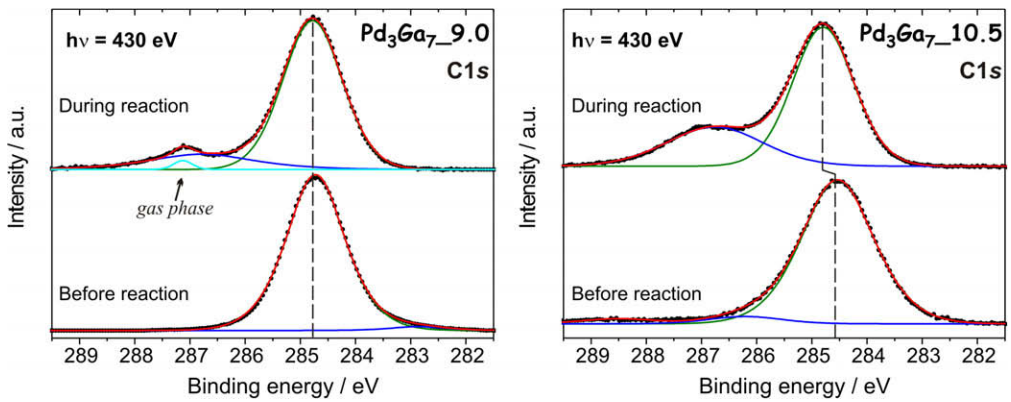

Fig. 7. C1*s* region of **Pd_3Ga_7_9.0** (left) and **Pd_3Ga_7_10.5** (right) before and during the hydrogenation of acetylene. In the upper-left spectrum the contribution of gas phase acetylene is exemplified.

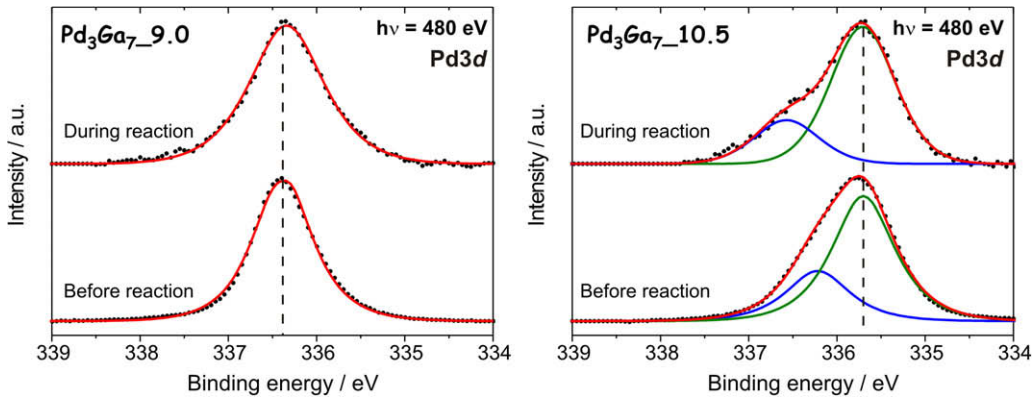

Fig. 8. Pd3*d* region for the etched samples **Pd_3Ga_7_9.0** (left) and **Pd_3Ga_7_10.5** (right) before and during the hydrogenation of acetylene.

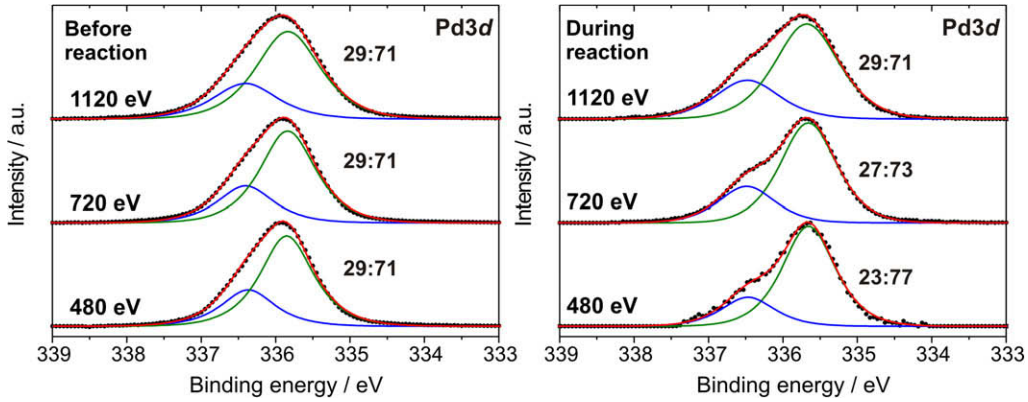

Fig. 9. Non-destructive depth profiling Pd3*d* XPS of **Pd_3Ga_7_10.5** before (left) and during (right) the hydrogenation of acetylene. The ratios of the different components are also given in the figure.

hydrogenation (Fig. 9). Neither additional components, nor significant changes of binding energies or component ratios were detected. The same high stability was observed for **Pd_3Ga_7_9.0**, which allows to differentiate between etched Pd–Ga intermetallic compounds and Pd metal. The latter forms an additional Pd component during alkyne hydrogenation, which was attributed to the formation of a carbon-containing palladium surface phase stable only *in situ*, i.e. in the presence of the alkyne feed [27–29]. Formation of this Pd–C phase provided the specificity of Pd being selective in alkyne hydrogenations. The Pd–C component possesses a higher binding energy (335.6 to 335.7 eV) than metallic Pd (335.0 eV). In the case of Pd–Ga intermetallic compounds the palladium 3*d* core level is already strongly modified: for the as-cast samples of PdGa and Pd_3Ga_7, binding energies of Pd3$d_{5/2}$ were 336.0 [1,30] and 336.4 eV, respectively. Thus, no further modification of Pd states by subsurface chemistry is necessary to obtain a selective catalyst. For **Pd_3Ga_7_10.5** the binding energy of the lower energy component is close to the binding energy of the Pd–C phase. Additionally, the covalent bonding between Pd and Ga makes the intermetallic compounds much more resistant against the incorporation of carbon or hydrogen atoms [1,3,30].

The investigation of the Ga3*d* region allows the determination of gallium oxidation states and the presence of Ga oxides on the surface (Fig. 10). The spectra show a resolvable Ga3*d* doublet at 18.5 and 19.0 eV and a broad component at higher binding energies. The binding energy of unresolved Ga3*d* doublet for metallic gallium is 18.5 eV, while for gallium intermetallic compounds slightly higher binding energies were reported: 18.7 eV for GaInSn [31] and 18.6 for Ni_2MnGa [32]. This allows us to unambiguously assign the observed doublet to Ga in an intermetallic compound. During the fitting of the spectra the ratio of Ga3$d_{3/2}$:Ga3$d_{5/2}$ was fixed to the theoretical value of 40:60 [15]. A successful fitting of the spectra was only possible when two additional components were introduced with binding energies of 20.0 eV and 20.7 eV. Since the area ratio and the energy difference of these components do not fit the spin-orbit split components of Ga3*d*, we attribute them to two different kinds of Ga oxides (two unresolved Ga3*d* doublets). Indeed, for Ga_2O and Ga_2O_3 similar binding energies of 20.0 eV and 21.0 eV, respectively, were reported [31,33,34]. Comparison of the samples revealed that the strongly etched sample contain more Ga oxides on the surface. Apparently, oxide layers are readily formed during contact of the freshly etched surface of Pd_3Ga_7 with air. During the reaction the relative concentration of oxidized gallium species increased. This can be explained by taking into account that the pressed samples were made from powders. The surface of the pill was cleaned by Ar^+ sputtering prior to XPS measurements; however, grain boundaries may contain significant amounts of oxygen, which can diffuse to the surface at 400 K. The surface Ga oxides overlayer is stable, even under much stronger reduction conditions (500 mbar of hydrogen at 573 K [4]), which explains why the surface Ga oxides were not reduced during the conditions applied in these studies. The segregation of oxygen may lead to the observed increase in Ga oxide coverage as well as the formation of oxygenated carbon species on the surface as was mentioned above.

The *in situ* XPS results are in good agreement with SEM/EDX data. The Pd3*d* XP spectra revealed that soft etching dissolves preferably Ga oxides preserving the intermetallic structure, while

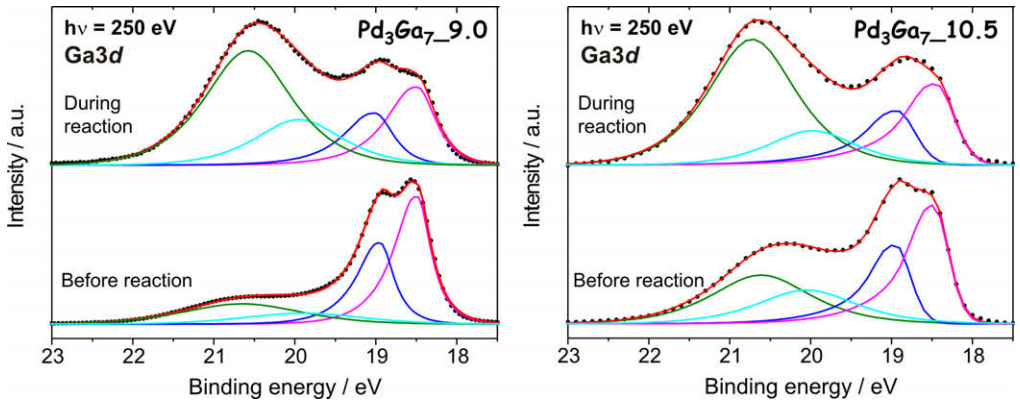

Fig. 10. XPS Ga3*d* region for etched samples **Pd_3Ga_7_9.0** (left) and **Pd_3Ga_7_10.5** (right), before and during the hydrogenation of acetylene.

strong etching leads to the partial destruction of the intermetallic compound and to the formation of a new surface phase with higher Pd-agglomeration. This surface phase readily accumulates carbon, thus reducing the long-term stability during acetylene hydrogenation. As expected, oxygen on the surface of Pd–Ga intermetallic compounds is bound to gallium and not to palladium.

3.7. Discussion

Intermetallic compounds exhibit high potential as selective hydrogenation catalysts. PdGa and Pd_3G_7 were selected based on knowledge of their crystal and electronic structures, applying the active-site isolation approach. Presence of the covalent bonding between gallium and palladium in these compounds was expected to diminish the sub-surface chemistry, known for elemental Pd [27–29], and to suppress the segregation phenomena, common for alloys [35]. Both chosen intermetallic compounds exhibit isolation of Pd atoms due to well-ordered crystal structure. It was shown that bulk structures of PdGa and Pd_3G_7 are stable during the reaction of acetylene hydrogenation and no incorporation of C and/or H atoms occurred (*in situ* XRD, *in situ* EXAFS and *in situ* Prompt Gamma Activation Analysis) [1,3,26]. XPS revealed that the electronic structures of the surface of PdGa and Pd_3Ga_7 are close to the electronic structures of the bulk, *e.g.* Pd *d*-band and the corresponding adsorption properties are strongly modified compared to elemental Pd [1,26,30].

The current study shows that gallium atoms on the surface of the intermetallic compounds PdGa and Pd_3Ga_7 are easily oxidized, and milling of the intermetallic compounds in air leads to the formation of a gallium oxides overlayer. This overlayer neither completely covers the surface, nor affects the Pd atoms, since the catalytic properties (high selectivity and long-term stability) of PdGa and Pd_3Ga_7 are preserved after milling [4]. We have demonstrated that chemical etching can be successfully applied to remove the gallium oxides overlayer partly, thus increasing the activity of the investigated intermetallic compounds. According to our results soft etching with ammonia solution (pH $\leqslant$ 9.0) is well suited for the removal, retaining the electronic structure of intermetallic compound as well as the isolation of palladium atoms on the surface. *In situ* XPS revealed perfect surface stability of the etched compounds during the reaction, thus, excluding sub-surface chemistry, such as segregation and/or incorporation of C/H atoms. In turn, strong etching (pH $\geqslant$10.0) leads to a significant destruction of the intermetallic surface and, therefore, to the breaking apart of the active-site isolation. The strong etching results in palladium-rich surfaces which are less selective than the softly etched intermetallic compounds, but still more selective and stable than supported palladium catalysts in the hydrogenation of acetylene.

It was shown that full removal of gallium oxides from the intermetallic surfaces cannot be achieved by chemical etching independent of the pH of the ammonia solution. Surface gallium oxides may play a role in hydrogen spillover as it was demonstrated for the supported Ga_2O_3–Pd/SiO_2 system [36]. In the case of Pd–Ga intermetallic compounds, surface palladium atoms are isolated from one another not only by gallium atoms but also by surface gallium oxides. Thus, hydrogen being dissociated on one Pd active site can become close to an acetylene molecule adsorbed on another Pd active site due to hydrogen spillover on the oxides. UHV single-crystal studies are expected to shed some light on the role of gallium in the semi-hydrogenation of acetylene catalyzed by Pd–Ga intermetallic compounds.

4. Conclusions

The drawback of the low surface area of PdGa and Pd_3Ga_7 intermetallic compounds – both perspective catalysts for the selective hydrogenation of acetylene – can be overcome by milling and chemical etching. Milling experiments showed that the presence of oxygen during the milling is necessary to prevent agglomeration of the particles. After milling, an etching procedure with ammonia solution was applied to increase the active surface area of the catalysts by removing the inactive gallium oxide overlayer. The chemical etching led to considerable, but not complete, removal of the oxides as well as to the formation of nano-sized caverns. This process optimizes the catalyst active surface by a combination of higher surface area, higher surface Pd concentration, and, possibly, by forming more active Pd ensembles. Etching at high pH values is accompanied by a partial destruction of the intermetallic crystal structure and the enrichment of the surface by palladium as detected by *in situ* XPS and SEM. This leads to a decrease in selectivity and long-term stability of the etched catalyst as is expected from the active-site isolation concept. Nonetheless, all etched PdGa and Pd_3Ga_7 catalysts still possess a significantly higher selectivity and long-term stability than Pd/Al_2O_3 after 20 h time on stream.

Acknowledgments

The authors express their gratitude to Dr. G. Auffermann for the chemical analysis, as well as to K. Klaeden and Dr. R.E. Jentoft for the BET measurements. We thank BESSY for providing beamtime and continuous support during the XPS experiments.

Appendix A. Supplementary data

Supplementary data associated with this article can be found, in the online version, at doi:10.1016/j.jcat.2009.03.007.

References

[1] K. Kovnir, M. Armbrüster, D. Teschner, T. Venkov, L. Szentmiklósi, F.C. Jentoft, A. Knop-Gericke, Yu. Grin, R. Schlögl, Surf. Sci. (2009), doi:10.1016/j.susc.2008.09.058.
[2] J. Osswald, R. Giedigkeit, M. Armbrüster, K. Kovnir, R.E. Jentoft, T. Ressler, Yu. Grin, R. Schlögl, European Patent EP/1834939A1, 2006.;
R. Giedigkeit, M. Armbrüster, K. Kovnir, Yu. Grin, R. Schlögl. J. Osswald, T. Ressler, R.E. Jentoft, International Patent WO/2007/104569 A1, 2007.
[3] J. Osswald, R. Giedigkeit, R.E. Jentoft, M. Armbrüster, F. Girgsdies, K. Kovnir, T. Ressler, Yu. Grin, R. Schlögl, J. Catal. 258 (2008) 210.
[4] J. Osswald, K. Kovnir, M. Armbrüster, R. Giedigkeit, R.E. Jentoft, U. Wild, Yu. Grin, R. Schlögl, J. Catal. 258 (2008) 219.
[5] K. Kovnir, J. Osswald, M. Armbrüster, R. Giedigkeit, T. Ressler, Yu. Grin, R. Schlögl, Stud. Surf. Sci. Catal. 162 (2006) 481.
[6] Yu. Grin, F.R. Wagner, M. Armbrüster, M. Kohout, A. Leithe-Jasper, U. Schwarz, U. Wedig, H.G. von Schnering, J. Solid State Chem. 179 (2006) 1707.
[7] A. Borodziński, G.C. Bond, Catal. Rev. 48 (2006) 91;
A. Borodziński, G.C. Bond, Catal. Rev. 50 (2008) 379.
[8] A.N.R. Bos, K.R. Westerterp, Chem. Eng. Process. 32 (1993) 1.
[9] P. Albers, J. Pietsch, S.F. Parker, J. Mol. Catal. A 173 (2001) 275.
[10] A.M. Doyle, Sh.K. Shaikhutdinov, H.-J. Freund, J. Catal. 223 (2004) 444.
[11] W.T. Tysoe, G.L. Nyberg, R.M. Lambert, J. Phys. Chem. 90 (1986) 3188.
[12] W. Palczewska, in: Z. Paal, P.G. Denon (Eds.), Hydrogen Effects in Catalysis, Marcel Decker, New York, 1988, p. 372.
[13] E. Hellner, F. Laves, Z. Naturforsch. A 2 (1947) 177.
[14] K. Khalaff, K. Schubert, J. Less-Common Met. 37 (1974) 129.
[15] D. Briggs, M.P. Seah, Practical Surface Analysis by Auger and X-ray Photoelectron Spectroscopy, Wiley, Chichester, 1988.
[16] H. Bluhm, M. Hävecker, A. Knop-Gericke, E. Kleimenov, R. Schlögl, D. Teschner, V.I. Bukhtiyarov, D.F. Ogletree, M. Salmeron, J. Phys. Chem. B 108 (2004) 14340.
[17] NIST Electron Inelastic Mean Free Path Database, version 1.1, <http://www.nist.gov/srd/nist71.htm>.
[18] C. Bryce, D. Berk, Ind. Eng. Chem. Res. 35 (1996) 4464.
[19] M.V. Lebedev, D. Ensling, R. Hunger, T. Mayer, W. Jaegermann, Appl. Surf. Sci. 229 (2004) 226.
[20] C.C. Chang, P.H. Citrin, B. Schwartz, J. Vac. Sci. Technol. 14 (1977) 943.
[21] D. Teschner, A. Pestryakov, E. Kleimenov, M. Hävecker, H. Bluhm, H. Sauer, A. Knop-Gericke, R. Schlögl, J. Catal. 230 (2005) 186.
[22] N.M. Rodriguez, P.E. Anderson, A. Wootsch, U. Wild, R. Schlögl, Z. Paál, J. Catal. 197 (2001) 365.
[23] Z. Paál, U. Wild, R. Schlögl, Phys. Chem. Chem. Phys. 3 (2001) 4644.
[24] D. Teschner, A. Pestryakov, E. Kleimenov, M. Hävecker, H. Bluhm, H. Sauer, A. Knop-Gericke, R. Schlögl, J. Catal. 230 (2005) 195.
[25] K. Kovnir, M. Schmidt, C. Waurisch, M. Armbrüster, Yu. Prots, Yu. Grin, Z. Kristallogr. NCS 223 (2008) 7.
[29] D. Teschner, Zs. Révay, J. Borsodi, A. Knop-Gericke, R. Schlögl, D. Milroy, S.D. Jackson, D. Torres, P. Sautet, Angew. Chem., Int. Ed. 47 (2008) 9274.
[27] D. Teschner, E. Vass, M. Hävecker, S. Zafeiratos, P. Schnörch, H. Sauer, A. Knop-Gericke, R. Schlögl, M. Chamam, A. Wootsch, A.S. Canning, J.J. Gamman, S.D. Jackson, J. McGregor, L.F. Gladden. J. Catal. 242 (2006) 26.
[28] D. Teschner, J. Borsodi, A. Wootsch, Zs. Révay, M. Hävecker, A. Knop-Gericke, S. David Jackson, R. Schlögl, Science 320 (2008) 86.
[29] D. Teschner, Zs. Révay, J. Borsodi, A. Knop-Gericke, R. Schlögl, D. Milroy, S.D. Jackson, D. Torres, P. Sautet, Angew. Chem., Int. Ed. 47 (2008) 9274.
[30] K. Kovnir, M. Armbrüster, D. Teschner, T.V. Venkov, F.C. Jentoft, A. Knop-Gericke, Yu. Grin, R. Schlögl, Sci. Technol. Adv. Mater. 8 (2007) 420.
[31] F. Scharmann, G. Cherkashinin, V. Breternitz, Ch. Knedlik, G. Hartung, Th. Weber, J.A. Schaefer, Surf. Interface Anal. 36 (2004) 981.
[32] C. Biswas, S.R. Barman, Appl. Surf. Sci. 252 (2006) 3380.
[33] R. Carli, C.L. Bianchi, Appl. Surf. Sci. 74 (1994) 99.
[34] C.C. Surdu-Bob, S.O. Saied, J.L. Sullivan, Appl. Surf. Sci. 183 (2001) 126.
[35] J.S. Sinfelt, Bimetallic Catalysts, Wiley, New York, 1983.
[36] S.E. Collins, D.L. Chiavassa, A.L. Bonivardi, M.A. Baltanás, Catal. Lett. 103 (2005) 83.